Dynamics of Hang Gliders

Guido de Matteis*
University of Rome "La Sapienza," Rome, 00184 Italy

In this paper, a general formulation for the analysis and simulation of the hang glider dynamics and control is presented. The hang glider is modeled as a compound system made of wing and pilot. Static stability criteria are reviewed for a typical, indicative configuration. The small-perturbation dynamic stability is investigated in the fixed and free control cases in analogy with the conventional aircraft. Unsteady aerodynamic effects are shown to play a role in the stability of the system.

Nomenclature

A = aspect ratio = b^2/S
b = wing span
C = Theodorsen function
C_D = drag coefficient
C_L = lift coefficient
C_l, C_m, C_n = aerodynamic moment coefficients
C_W = weight coefficient
$\bar{c}$ = reference chord
F = control force
F_A = aerodynamic force
F_l = longitudinal control force, normal to S-P
F_n = lateral control force
g = acceleration of gravity
h_d = deformation component of the momentum
I = inertia matrix
k = reduced frequency
L, M, N = aerodynamic moment components
l_s = length of suspension
M = aerodynamic moment
m = mass
p, q, r = angular velocity components
R = position vector
S = reference area
s = Laplace variable
u, v, w = velocity components
u_α = $-(\cos\alpha_e u_e + \sin\alpha_e w_e)/\sin\alpha_e$
V = flight speed
v = velocity vector
W = weight
w_α = $(\cos\alpha_e u_e + \sin\alpha_e w_e)/\cos\alpha_e$
X, Y, Z = aerodynamic force components
X_1, X_2 = state vectors
x, y, z = coordinates in F_B
α = angle of attack
β = sideslip angle
γ = glide angle
δ, σ = longitudinal and lateral control angles
ϵ = twist angle
ζ = damping
θ, ϕ, ψ = Euler angles
κ = mass ratio, m/m^T
Λ = sweep angle
λ = taper ratio
μ = mass density
ξ, η = coordinates in F_s
Φ = control vector
ω = frequency
ω = angular velocity vector

Subscripts
C, O, S = characteristic points
c.g. = center of gravity
e = equilibrium
s = section
st = steady state

Superscripts
C, O, S = characteristic points
P = pilot
T = total
W = wing
$\hat{}$ = dimensionless
$-$ = Laplace transformed quantity
$'$ = perturbation variable

I. Introduction

THE dynamics and control of hang gliders is the subject of this study. These apparently simple machines still present considerable difficulties when their more complex simulations are dealt with. Development of hang gliders on a semiempirical base led to several problems connected with their safe performance and, although the pertinent literature is—at this time—rather large, a complete and rigorous analysis in terms of dynamic response of the system is still missing.

As is well known, a hang glider is a tail-less vehicle controlled by shifting the pilot's weight longitudinally and laterally. Control effectiveness demands a large longitudinal variation of c.g. position and a significant vertical distance between this point and the aerodynamic center. The lifting surface, usually made of fabric, stiffened by battens, is flexible and the hang-glider structure, made by a number of tubes (leading edges, keel, cross tube), rigging, and cables, is largely subjected to elastic deformations under the action of the aerodynamic loads. Furthermore, due to the variable position of the pilot, the geometrical configuration of the vehicle and its mass distribution depend on the trimmed flight conditions, even in the case of a rigid structure. Yet, an overall mass m less than 100 kg and a cruise velocity V of the order of 10 m/s determine, in a typical case, a relative density $\mu = 2m/\rho\bar{c}S$ lower than 10 and a value of the reduced frequency $k = \bar{c}\omega/2V$ as high as 0.4, where $\bar{c}$ is the reference chord, S is the wing surface, and ω is a characteristic frequency of oscillation. As a result, when one analyzes unsteady aerodynamic effects, the apparent additional mass is of the same order of magnitude as the glider itself, and the unsteady circulatory lift effects are not negligible in determining the dynamic behavior of the system.

Received April 6, 1990; revision received Sept. 21, 1990; accepted for publication Oct. 2, 1990.

*Research Scientist, Department of Mechanics and Aeronautics, via Eudossiana, 18. Member AIAA.

We should point out that most of the above features are rather unusual in classical aircraft flight mechanics. This makes any attempt to formulate and develop a sufficiently general model for the prediction of the vehicle performance and control response more cumbersome and difficult.

With this in mind some significant studies among the available literature are now briefly recalled. The steady-state performances of a number of hang gliders are analyzed and discussed in Ref. 1. The basic criteria of static stability (stability with force, stability with displacement) are outlined. The very different behaviors of different machines is emphasized through the analysis of a large amount of wind-tunnel data. Instabilities are shown to occur in certain critical flight phases, and conclusions are drawn on the favorable effects, in terms of stability, of the fabric flexibility. On the other hand, the aeroelastic deformations of the tubular structure have uncertain effects on the system static stability. A very comprehensive analysis of hang gliders is presented in Ref. 2. Interesting conclusions are provided in different areas such as aerodynamics and aeroelasticity, performances particularly in turning flight, unsteady aerodynamics, dynamics, and wind-tunnel testing of elastically scaled models. Again it is stressed how the complex phenomena involved in many of the fields indicated above prevent the application of common use approximations for conventional aircraft. When we focus on the flight dynamics and control section in Ref. 2, small-perturbation solutions are given in the so-called fixed trapeze case, i.e., the pilot is rigidly linked to the wing—its position depending on the equilibrium of the steady flight—and constantly lies in the plane of symmetry. For this situation, the classical short period and phugoid modes result, and some qualitative considerations on the effects of the unsteady aerodynamics on the related characteristic roots are provided.

As was recommended at the end of Ref. 2, a complete formulation of the dynamics of the system should account for the flexible coupling of pilot and glider. This kind of model was developed in Ref. 3 by simulating the hang glider as a compound system made of wing and pilot. In particular, by writing the equations of motion for the complete system and for a subsystem consisting of the pilot and his harness, a quite general model is given that appears suitable for a number of applications. In this respect, in the cited report, the linearized equations of longitudinal and lateral motion are developed for the evaluations of the corresponding state functions $X_1 = (u', w', \theta', \delta')$ and $X_2 = (\beta', p', r', \phi', \sigma')$, where δ' and σ' are the longitudinal and lateral perturbation control angles, respectively, as a function of the control forces F_l' and F_n' (Fig. 1) and time, for a typical, conventional glider configuration. There, as a preliminary application, the free-trapeze stability is discussed in analogy with the free-stick control of the airplane. Unsteady aerodynamic stability derivatives are calculated by a modified-strip-line theory approach[4] that relies on the work[5] for the mathematical expression of the aerodynamic transfer function $C(k)$.

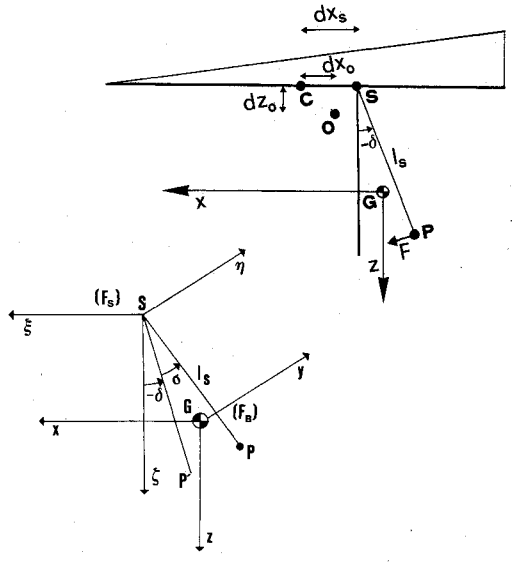

Fig. 1 Sketch of the problem.

This paper deals with some aspects of the dynamics of a hang glider whose motion is simulated by the above compound-system model. The glider is assumed to be rigid, under the hypothesis that the aeroelastic effects on its structure can eventually be dealt with by an appropriate evaluation of the velocity dependence of the aerodynamic derivatives. In Sec. II, the proposed formulation is outlined and discussed; then in Secs. III and IV a number of applications are carried out that show the effects of characteristic parameters on the stability in the circumstances of fixed and free trapeze. It is shown that the trimmed flight condition can severely affect the stability as a consequence of the large variation of the position of the c.g. involved. The noticeable effects of flow unsteadiness are confirmed and appear to favorably contribute to increase the stability of the system.

II. Formulation

The basic set of equations governing the motion of the glider was discussed in detail in Ref. 3 and will be only briefly recalled here. Reference is made to Fig. 1 for the sketch of the problem considered. The equations of the complete system made of pilot and wing are written in body axes (F_B) with origin in the c.g., the location of which depends on the pilot's position. We have

$$m^T(\dot{v} + \tilde{\omega}v) = F_A^W + F_A^P + W^W + W^P \tag{1}$$

$$I\dot{\omega} + I\dot{\omega} + \tilde{\omega}I\omega + \dot{h}_d = M_C^W + \tilde{R}_C F_A^W + \tilde{R}_P F_A^P \tag{2}$$

where h_d is the deformation component of the momentum,[6] and we have

$$\dot{h}_d = m^W(\tilde{R}_O\ddot{R}_O + \tilde{\omega}\tilde{R}_O\dot{R}_O) + m^P(\tilde{R}_P\ddot{R}_P + \tilde{\omega}\tilde{R}_P\dot{R}_P)$$

In the above equations, R_O, R_C, and R_P are the position vectors of the following points: O the center of mass of the wing, C the intersection of the cross tube and the keel, and P the center of mass of the pilot. They are given by

$$R_C = -[1/(m^W + m^P)][m^W R_{O_1} + m^P(R_{S_1} + R_P^S)] \tag{3}$$

$$R_O = R_C + R_{O_1} \tag{4}$$

$$R_P = R_C + R_{S_1} + R_P^S \tag{5}$$

where

$$R_{O_1} = \begin{vmatrix} -dx_O \\ 0 \\ dz_O \end{vmatrix}, \quad R_{S_1} = \begin{vmatrix} -dx_S \\ 0 \\ dz_S \end{vmatrix}, \quad R_P^S = L_{BP}\begin{vmatrix} 0 \\ 0 \\ l_S \end{vmatrix} \tag{6}$$

$$L_{BP} = \begin{vmatrix} \cos\delta & 0 & \sin\delta \\ -\sin\sigma\sin\delta & \cos\delta & \sin\sigma\cos\delta \\ -\cos\sigma\sin\delta & -\sin\delta & \cos\sigma\cos\delta \end{vmatrix} \tag{7}$$

Moreover,

$$W = gL_{BI}\begin{vmatrix} 0 \\ 0 \\ m^W + m^P \end{vmatrix}, \quad F_A = \begin{vmatrix} X \\ Y \\ Z \end{vmatrix}, \quad M = \begin{vmatrix} L \\ M \\ N \end{vmatrix} \tag{8}$$

where X, Y, and Z are the axial, lateral, and normal aerodynamic forces and $\boldsymbol{L}_{BI}$, $\boldsymbol{v}$, $\boldsymbol{\omega}$, and the operator $\sim$ have the usual meaning,[6] $\boldsymbol{L}_{BI}$ being the transformation matrix from the inertial frame to F_B.

The motion of the pilot subsystem is modeled by taking a reference frame F_S constantly equioriented with respect to F_B and centered in S, the point of suspension of the pilot. By assuming that the c.g. of the subsystem is in P, we obtain the following moment equation:

$$I^P\ddot{\Phi} = \tilde{\boldsymbol{R}}_P^S\{(\boldsymbol{W}^P + \boldsymbol{L}_{BP}\boldsymbol{F} + \boldsymbol{F}_A) - m^P[(\dot{\boldsymbol{v}} + \ddot{\boldsymbol{R}}_S + \tilde{\boldsymbol{\omega}}\boldsymbol{v}) - 2\tilde{\boldsymbol{R}}_P^S\boldsymbol{\omega} + \tilde{\boldsymbol{\omega}}\tilde{\boldsymbol{\omega}}\boldsymbol{R}_P^S]\} - I^P\dot{\boldsymbol{\omega}} \tag{9}$$

with

$$\boldsymbol{R}_S = \boldsymbol{R}_C + \boldsymbol{R}_{S_1}, \qquad \boldsymbol{\Phi} = \begin{vmatrix} \sigma \\ \delta \\ 0 \end{vmatrix}, \qquad \boldsymbol{F} = \begin{vmatrix} F_l \\ F_n \\ 0 \end{vmatrix} \tag{10}$$

where $\boldsymbol{F}_A^P$ is the aerodynamic force on the pilot and $\boldsymbol{\Phi}$ is the control variables vector.

In order to solve the small-disturbance dynamics of the system, Eqs. (1), (2), and (9) are linearized about a reference condition of steady rectilinear flight in the plane of symmetry $0xy$. In the linearization the following definitions are used:

$$\begin{aligned} u' &= u - u_e, \quad v' = v, \quad w' = w - w_e \\ \theta' &= \theta - \theta_e, \quad \phi' = \phi, \quad \psi' = \psi \\ p' &= p, \quad q' = q, \quad r' = r \\ \delta' &= \delta - \delta_e, \quad \sigma' = \sigma \\ F_l' &= F_l - F_{l_e}, \quad F_n' = F_n \end{aligned} \tag{11}$$

For a detailed derivation of the linearized equations, see Ref. 3.

Next the linearized equations are recast in dimensionless form, where the reference variables are the standard ones in flight dynamics.[6] Finally, after taking the Laplace transform, the motion and control equations are written for the longitudinal and lateral case, respectively:

$$\boldsymbol{A}_1\overline{\boldsymbol{X}}_1 = \boldsymbol{B}_1 \tag{12}$$

Table 1 Coefficients of the small-perturbation Laplace transformed equations

$$\boldsymbol{A}_1 = \begin{bmatrix} -\left(2\mu - \frac{C_{x_{\dot\alpha}}}{\hat u_\alpha}\right)\hat s + \frac{C_{x_\alpha}}{\hat u_\alpha} + 2C_{x_e}\hat u_e & \frac{C_{x_{\dot\alpha}}}{\hat w_\alpha}\hat s + \frac{C_{x_\alpha}}{\hat w_\alpha} + 2C_{x_e}\hat w_e & -C_{W_e}\cos\theta_e + (-2\mu\hat w_e + C_{x_q})\hat s & 0 \\ \frac{C_{z_{\dot\alpha}}}{\hat u_\alpha}\hat s + \frac{C_{z_\alpha}}{\hat u_\alpha} + 2C_{z_e}\hat u_e & -\left(2\mu - \frac{C_{z_{\dot\alpha}}}{\hat w_\alpha}\right)\hat s + \frac{C_{z_\alpha}}{\hat w_\alpha} + 2C_{z_e}\hat w_e & -C_{W_e}\sin\theta_e + (2\mu\hat u_e + C_{z_q})\hat s + C_{z_{\dot q}}\hat s^2 & 0 \\ \frac{\hat z_e^C C_{x_{\dot\alpha}} - \hat x_e^C C_{z_{\dot\alpha}} + 2C_{m_{\dot\alpha}}}{2\hat u_\alpha}\hat s + \frac{1}{2\hat u_\alpha}\left(\hat z_e^C C_{x_\alpha}^W - \hat x_e^C C_{z_\alpha}^W + \hat z_e^P C_{x_\alpha}^P - \hat x_e^P C_{z_\alpha}^P + 2C_{m_\alpha}^W\right) + \hat u_e\left(\hat z_e^C C_{x_e}^W - \hat x_e^C C_{z_e}^W + \hat z_e^P C_{x_e}^P - \hat x_e^P C_{z_e}^P + 2C_{m_e}^W\right) & \frac{\hat z_e^C C_{x_{\dot\alpha}} - \hat x_e^C C_{z_{\dot\alpha}} + 2C_{m_{\dot\alpha}}}{2\hat w_\alpha}\hat s + \frac{1}{2\hat w_\alpha}\left(\hat z_e^C C_{x_\alpha}^W - \hat x_e^C C_{z_\alpha}^W + \hat z_e^P C_{x_\alpha}^P - \hat x_e^P C_{z_\alpha}^P + 2C_{m_\alpha}^W\right) + \hat w_e\left(\hat z_e^C C_{x_e}^W - \hat x_e^C C_{z_e}^W + \hat z_e^P C_{x_e}^P - \hat x_e^P C_{z_e}^P + 2C_{m_e}^W\right) & -\left(\hat I_y + \hat x_e^C C_{z_{\dot q}} - 2C_{m_{\dot q}}\right)\hat s^2 + \frac{1}{2}\left(\hat z_e^C C_{x_q}^W - \hat x_e^C C_{z_q}^W + \hat z_e^P C_{x_q}^P - \hat x_e^P C_{z_q}^P + 2C_{mq}\right)\hat s & \hat l_s\left\{\sin\delta_e\left[\left(\kappa^P C_{x_e}^W - \kappa^W C_{x_e}^P\right)/2 - \left(\hat x_e^P\mu^P\kappa^W - \hat x_e^O\mu^W\kappa^P\right)\hat s^2\right] + \cos\delta_e\left(\kappa^P C_{z_e}^W - \kappa^W C_{z_e}^P\right)/2 - \left(\hat z_e^P\mu^P\kappa^W - \hat z_e^O\mu^W\kappa^P\right)\hat s^2\right]\right\} \\ -\mu^P\frac{\hat l_s}{2}\cos\delta_e\hat s + \frac{\hat l_s}{2}\left\{2\left(\cos\delta_e C_{x_e}^P - \sin\delta_e C_{z_e}^P\right)\hat u_e + \frac{1}{\hat u_\alpha}\left(\cos\delta_e C_{x_\alpha}^P - \sin\delta_e C_{z_\alpha}^P\right)\right\} & -\mu^P\frac{\hat l_s}{2}\sin\delta_e\hat s + \frac{\hat l_s}{2}\left\{2\left(\cos\delta_e C_{x_e}^P - \sin\delta_e C_{z_e}^P\right)\hat w_e + \frac{1}{\hat w_\alpha}\left(\cos\delta_e C_{x_\alpha}^P - \sin\delta_e C_{z_\alpha}^P\right)\right\} & -C_W^P\frac{\hat l_s}{2}\cos(\delta_e + \theta_e) - \frac{\hat l_s}{2}\mu^P(\cos\delta_e\hat w_e + \sin\delta_e\hat u_e)\hat s - \hat I_\eta^P\hat s^2 & -(\hat I_\eta^P - \kappa^P\mu^P\hat l_s^2)\hat s^2 - \frac{\hat l_s}{2}\left[C_W^P\cos(\delta_e + \theta_e) + \sin\delta_e C_{x_e}^P + \cos\delta_e C_{z_e}^P\right] \end{bmatrix}$$

$$\boldsymbol{A}_2 = \begin{bmatrix} -2\mu\hat s + C_{y_\beta} & C_{y_p} + \frac{2\mu}{A}\sin\alpha_e & C_{y_r} - \frac{2\mu}{A}\cos\alpha_e & C_W\cos\theta_e & 0 \\ C_{l_\beta} - \frac{1}{2A}\left(\hat z_e^C C_{y_\beta}^W + \hat z_e^P C_{y_\beta}^P\right) & -A\hat I_x\hat s + C_{l_p} - \frac{1}{2A}\left(\hat z_e^C C_{y_p}^W + \hat z_e^P C_{y_p}^P\right) & A\hat I_{xz}\hat s + C_{l_r} - \frac{1}{2A}\left(\hat z_e^C C_{y_r}^W + \hat z_e^P C_{y_r}^P\right) & 0 & \frac{\hat l_s}{A}\cos\delta_e\left[\left(-C_{z_e}^W\kappa^W + C_{z_e}^P\kappa^P\right)/2 - \left(\mu^W\kappa^P\hat z_e^O - \mu^P\kappa^W\hat z_e^P\right)\hat s^2\right] \\ C_{n_\beta} - \frac{1}{2A}\left(\hat x_e^C C_{y_\beta}^W + \hat x_e^P C_{y_\beta}^P\right) & -A\hat I_{xz}\hat s + C_{n_p} + \frac{1}{2A}\left(\hat x_e^C C_{y_p}^W + \hat x_e^P C_{y_p}^P\right) & -A\hat I_z\hat s + C_{n_r} + \frac{1}{2A}\left(\hat x_e^C C_{y_r}^W + \hat x_e^P C_{y_r}^P\right) & 0 & \frac{\hat l_s}{A}\cos\delta_e\left[\left(C_{x_e}^W\kappa^W + C_{z_e}^P\kappa^P\right)/2 - \left(\mu^P\kappa^W\hat x_e^P - \mu^W\kappa^P\hat x_e^O\right)\hat s^2\right] \\ 0 & \frac{1}{A} & \frac{1}{A}\tan\theta_e & -\hat s & 0 \\ \frac{\mu^P}{A^2}\hat l_s\cos\delta_e\hat s - \frac{\hat l_s}{2A}\cos\delta_e C_{y_\beta}^P & -A\hat I_\xi^P\hat s - \frac{\hat l_s}{2A}\cos\delta_e\left(C_{y_p}^P + \frac{2}{A}\mu^P\hat w_e\right) & \frac{\hat l_s}{2A}\cos\delta_e\left(-C_{y_r}^P + \frac{2}{A}\mu^P\hat u_e\right) & -\frac{\hat l_s}{2A}C_W^P\cos\theta_e\cos\delta_e & -\left(A^2\hat I_\xi^P + \frac{\kappa}{A}\mu^P\hat l_s^2\cos^2\delta_e\right)\hat s^2 + \frac{\hat l_s}{2A}\cos\delta_e\left(C_W^P\cos\theta_e + C_{z_e}^P\right) \end{bmatrix}$$

Table 2 Characteristic parameters of the hang glider

$S = 16.7$ m^2	$b = 10$ m	$\lambda = 0.4$	$A = 6$
$\epsilon = -11$ deg	$\Lambda_{c/4} = 25$ deg	$c_r = 2.38$ m	$\bar{c} = 1.67$ m
$dz_S = 0$	$dx_O = 0.36$ m	$dz_O = 0.05$ m	$l_s = 1.27$ m
$I^W_{S_x} = 84.1$ kg m^2	$I^W_{S_y} = 27.5$ kg m^2	$I^W_{S_z} = 111.6$ kg m^2	

$$A_2\bar{X}_2 = B_2 \tag{13}$$

where

$$B_1^T = (0,\ 0,\ 0,\ 0.5\ \hat{l}_S\bar{\bar{F}}_l')$$

$$B_2^T = (0,\ 0,\ 0,\ 0,\ 0.5\ \cos\delta_e\bar{\bar{F}}_n/A)$$

The state vectors are now relative to dimensionless variables, and A_1, A_2 are given in Table 1. The moments of inertia in the above equations are reported in Appendix A as a function of the equilibrium variables. In deriving Eqs. (12) and (13), the flight speed derivatives that should account for the aeroelastic effects (C_{x_V}, C_{z_V}, and C_{m_V}) were all set to zero. The aerodynamics of the wing is dealt with by a lifting-line model, whose accuracy is within the simplifying assumptions involved in the present analysis. The section moment coefficient and zero-lift angle were evaluated by a two-dimensional sail model[7] for a flexible profile having a 5% slack. Because of the rather complex structure of the hang glider in terms of parasite drag prediction and the poor characteristics of the above aerodynamic model for the evaluation of the induced drag of the wing, the drag polar of the glider was expressed in the following data-fit form[2]:

$$C_D = C_{D_{\min}} + h(C_L - C_{L_0})^2 \tag{14}$$

with $C_{D_{\min}} = 0.073$, $h = 0.138$, and $C_{L_0} = 0.27$, used in the range $0.2 < C_L < 1.1$.

Turning to the pilot's aerodynamics, the lift and moment were neglected, whereas $S^P C_D^P = 0.11$ m^2 and 0.55 m^2 for a pilot in prone position and for a seated pilot, respectively, where S^P is a reference area.[1] By the lifting-line model together with Eq. (14), the steady-state aerodynamic coefficients and stability derivatives were determined as a function of the glider angle of attack α. In the evaluation of the so-called rotary derivatives (p, q, r derivatives), the actual position of the c.g., as resulting from the steady equilibrium at a given α, was taken as the center of rotation.

The evaluation of the effects of the unsteady aerodynamics in terms of stability derivatives, limited to the longitudinal motion, discussed in Ref. 3, is recalled in Appendix B. It is worth noting that, as it will be seen later, due to the frequency-dependent character of these derivatives when flow unsteadiness is taken into consideration, some additional complexity may arise in the analysis of the free oscillations of the system.

III. Steady-State Solutions and Static Stability

A reference conventional configuration of a hang glider is treated in what follows, and its characteristics are summarized in Table 2. By solving Eqs. (1), (2), and (9) in a situation of steady, rectilinear flight in the plane of symmetry, we obtain the results reported in Fig. 2, where the glide angle γ (Fig. 2a),

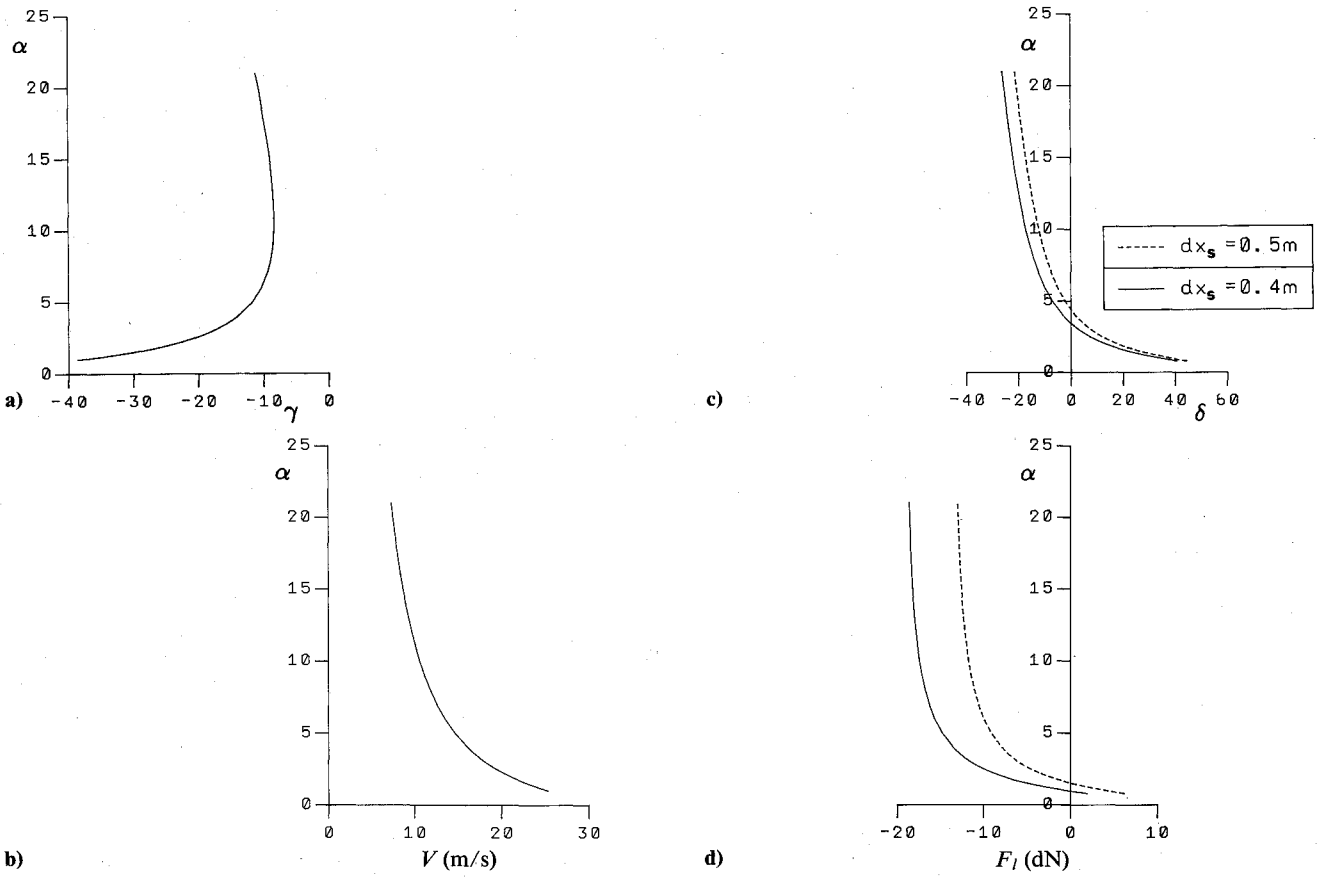

Fig. 2 Steady state solutions: a) glide angle vs α; b) velocity vs α; c) control angle vs α; and d) longitudinal control force vs α.

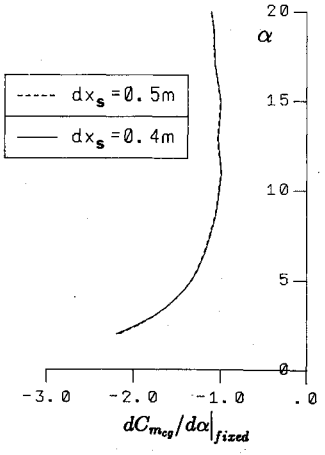

Fig. 3 Static longitudinal stability: pitch stiffness vs α.

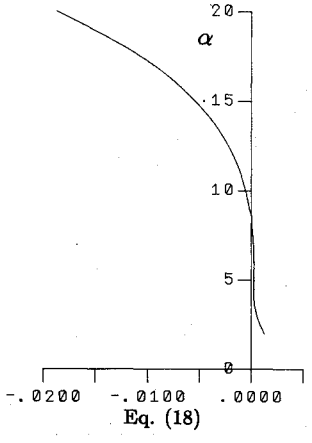

Fig. 4 Static lateral stability criterion vs α.

the velocity V (Fig. 2b), the control angle δ (Fig. 2c), and the control force F_l (Fig. 2d) are given vs α for the considered glider. The figures show that the requirements of static stability for a hang glider, as stated by Ref. 1, namely positive stability with displacement $[d(-\delta)/d\alpha>0]$ and positive stability with force $[d(-F_l)/d\alpha>0]$, are all met. Figures 2c and 2d also report the effect of a backward displacement of the suspension point of the pilot on δ and F_l. As expected, the control force is largely reduced for a corresponding small variation of δ. The pitch stiffness is evaluated by

$$\left.\frac{dC_{m_{c.g.}}}{d\alpha}\right|_{fixed} = 2C^W_{m_\alpha} - \hat{x}^C(\delta)C^W_{z_\alpha} + \hat{z}^C(\delta)C^W_{x_\alpha} - \hat{x}^P(\delta)C^P_{z_\alpha} + \hat{z}^P(\delta)C^P_{x_\alpha} \tag{15}$$

and Fig. 3 shows that wide variations of this parameter vs α are to be considered due to the large displacement of the c.g. necessary for trimming, whereas the effect of the suspension point is negligible.

The condition of steady flight with free controls, i.e., with $F_l = 0$, is also to be investigated since it provides the equilibrium values for the free-trapeze dynamic analysis. In this respect, we obtain $\alpha_{free} = 1$ deg for $dx_s = 0.4$ m and $\alpha_{free} = 1.5$ deg for $dx_s = 0.5$ m. The corresponding values of the control angle are $\delta_{free} = 35$ deg and $\delta_{free} = 25.6$ deg.

The pitch stiffness, free trapeze is

$$\left.\frac{dC_{m_{c.g.}}}{d\alpha}\right|_{free} = \left.\frac{dC_{m_{c.g.}}}{d\alpha}\right|_{fixed} - \left(C^W_z\frac{\partial\hat{x}^C}{\partial\delta} - C^W_x\frac{\partial\hat{z}^C}{\partial\delta} + C^P_z\frac{\partial\hat{x}^P}{\partial\delta} - C^P_x\frac{\partial\hat{z}^P}{\partial\delta}\right)\left.\frac{d\delta}{d\alpha}\right|_{free} \tag{16}$$

In Eq. (16), $d\delta/d\alpha|_{free}$ is obtained by numerical differentiation of the following expression:

$$\delta(\alpha)|_{free} = \tan^{-1}\left(-\tan\theta + \frac{C^P_x}{C^P_W\cos\theta}\right) \tag{17}$$

where $C^P_z \sin\delta$ has been neglected with respect to $C^P_x \cos\delta$. By solving Eq. (16) for the above free-control angles of attack, we have $dC_{m_{c.g.}}/d\alpha|_{free} = -2.5$ for $dx_s = 0.4$ m and $dC_{m_{c.g.}}/d\alpha|_{free} = -0.6$ for $dx_s = 0.5$ m. Therefore, a backward displacement of the suspension point appears to have negative effects on the free-control stability since the free-control static margin is reduced by shifting back the c.g. We should also note that $\delta_{free} = 25.6$ deg is already beyond the geometric limits of the displacement of the pilot acting on the control bar, which is given, with some approximation, by $14 \text{ deg} < \delta < -48$ deg for $l_s = 1.2$ m in the present case.

Turning now to the lateral motion, the hang-glider criterion for lateral static stability as derived from the zero-order coefficient of the characteristic polynomial of the matrix A_2 is

$$\left[C_{l_\beta} - \frac{1}{2A}(z^C_e C^W_{y_\beta} + z^P_e C^P_{y_\beta})\right]\left[\left(C_{n_r} + \frac{x^C_e}{2A}C_{y_r}\right)\cos\theta_e - \left(C_{n_p} + \frac{x^C_e}{2A}C_{y_p}\right)\frac{\sin\theta_e}{A}\right] + \left[C_{n_\beta} - \frac{1}{2A}(x^C_e C^W_{y_\beta} + x^P_e C^P_{y_\beta})\right] \times \left[\left(C_{l_p} - \frac{z^C_e}{2A}C_{y_p}\right)\frac{\sin\theta_e}{A} - \left(C_{l_r} - \frac{z^C_e}{2A}C_{y_r}\right)\cos\theta_e\right] > 0 \tag{18}$$

In Fig. 4, the reported variation of the lateral stability with α shows that inequality (18) is satisfied only for $\alpha < 8$ deg, which means that a diverging spiral motion would possibly occur in a large part of the flight envelope. This is discussed in the following section. Additional information on the lateral stability characteristics of the modeled glider is provided in Table 3 in a reference condition corresponding to $\alpha_e = 14$ deg.

Table 3 Stability derivatives for the lateral dynamics

$C^W_{y_\beta} = -0.037$	$C^W_{y_p} = 0.230$	$C^W_{y_r} = 0.015$
$C^P_{y_\beta} \cong -C^P_D$	$C^P_{y_p} = 0$	$C^P_{y_r} = 0$
$C_{l_\beta} = -0.137$	$C_{l_p} = -0.840$	$C_{l_r} = 0.072$
$C_{n_\beta} = 0.034$	$C_{n_p} = -0.370$	$C_{n_r} = -0.027$

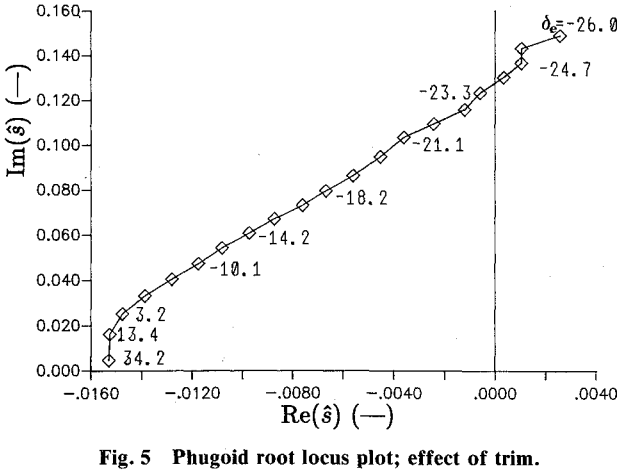

Fig. 5 Phugoid root locus plot; effect of trim.

Table 4 Effects of pilot's weight and drag on stability

m, kg	C_d	δ	V, m/s	γ	SP	PH
70	0.0069	−21.1	9.3	8.7	$-0.36 \pm 0.28i$	$-0.0036 \pm 0.10i$
45	0.0069	−23.4	7.7	8.7	$-0.45 \pm 0.24i$	$-0.0034 \pm 0.12i$
70	0.0340	−21.4	9.0	10.2	$-0.36 \pm 0.28i$	$-0.0079 \pm 0.10i$

IV. Dynamic Stability

Longitudinal Motion

The fixed-trapeze stability is dealt with by eliminating the control equation, dropping the variable δ', and setting the control force equal to zero in Eq. (12). The eigenvalues of the reduced, homogeneous system are obtained by solving the classical characteristic quartic equation in terms of the Laplace variable $\hat{s}$. The case with no unsteady aerodynamic effects will be discussed first as a reference solution.

We observe that the well-known short-period (SP) and phugoid roots (PH) characterize the free oscillations of the hang glider in analogy with the conventional aircraft. The latter mode is significantly affected by the trim conditions. This is shown in Fig. 5, where the effect of the control angle δ_e on the phugoid eigenvalues is reported. A backward equilibrium position of the pilot reduces the stability and, for negative values of δ_e as large as -24 deg, the motion is divergent. The same effect is obtained by shifting back the suspension point so that, for $dx_s = 0.5$ m, the real part of $\hat{s}$ is already positive at $\delta_e = -19$ deg. This is consistent with the results in Ref. 2, where the same effects are observed as the trim lift coefficient is increased. Figure 6 reports the effect of trim on the dimensionless short-period roots. A noticeable reduction of the damping appears in the range $13 \text{ deg} < \delta_e < -10$ deg, related to the values of the pitch damping coefficient that decreases as α grows. In any case, the damping remains high ($t_{\text{half}} = 0.26$ s at $\delta_e = -22$ deg), whereas a slight variation of the frequency may be observed in the figure.

A sensitivity analysis should include the effects of the pilot's weight and drag. In this respect some indicative results are shown in Table 4. The angle of attack is 14 deg in the three cases: a significant effect is that of the C_D^P on the phugoid roots, where an increase in damping of 98% is observed for a seated pilot with respect to a prone one.

When we expand the 4×4 determinant of A_1 given in Table 1, the characteristic equation of the sixth order for the free-trapeze system results. The eigenvalues are calculated at the values of α_{free} given in the previous section for the two cases of $dx_s = 0.4$ and 0.5 m. Figure 7 reports the roots relative to two periodic motions. The analysis shows that the deformation of the system plays a relevant role through the $\dot{h}_d$ term in the linear momentum equation. In this respect, two aperiodic modes occur, namely $\hat{s} = -11.5$ and -0.62 for $dx_s = 0.4$ m and $\hat{s} = 1$ and -0.59 for $dx_s = 0.5$ m. If the deformation component of the momentum were neglected, we would obtain a high-frequency, highly damped motion. The present results may be taken as qualitative, due principally to the simple aerodynamics involved and since aeroelastic deformations were neglected. However, they show that highly divergent motions can appear is a situation that corresponds to the real case of a pilot unable to any action on the control bar.

When the free oscillations of the system are analyzed in the presence of unsteady aerodynamic effects, the following characteristic equation results for the fixed-trapeze case:

$$\sum_{N=0}^{4} C_N(i\hat{\omega})\hat{s}^N = 0 \tag{19}$$

where $\hat{s} = \hat{n} + i\hat{\omega}$ and the coefficients C_N depend on the reduced frequency since $\hat{\omega} = k$. Equation (19) is solved by iterating from an initial value of $\hat{\omega}$, i.e., the one corresponding to the short-period or phugoid frequency in the quasistatic approach, until a converged solution is obtained. Figure 8 shows the values of the unsteady stability derivatives in the actual range of the reduced frequency as computed by the method reported in Appendix B. The problem was solved for $\alpha = 14$ deg, which is representative of a standard cruise flight condition. When the effects of the single derivatives on the stability are considered, the value of $C_{z_{\dot{\alpha}}}$ is crucial for the short-period mode in the sense that, by operating on the mass of the system in the term $(2\mu - C_{z_{\dot{\alpha}}}/\hat{\omega}_\alpha)$, reduces the frequency and increases the damping up to a point where no converged solution is obtained and the short period appears no longer to exist. Turning to the phugoid mode, we observe a quite small increase of the frequency (<1%) and a rather large increase of the damping, which raises from $\zeta = 0.035$ to $\zeta = 0.90$. Again, an analysis of the approximate solutions of the phugoid motion shows that this relevant effect is caused by the negative value of $C_{z_{\dot{\alpha}}}/\hat{u}_\alpha$ in the $\partial C_z/\partial\hat{u}$ term of the Z-force equation of motion, whereas the total mass variation due to the contribution of $C_{x_{\dot{\alpha}}}$ in the $(2\mu - C_{x_{\dot{\alpha}}}/\hat{u}_\alpha)$ term of the X-force equation is negligibly small.

As for the free-control case (Fig. 7), we observe the following: the low-frequency roots present a small variation, namely from $\hat{s} = -0.016 \pm 0.0061i$ to $\hat{s} = -0.016 \pm 0.0062i$ when the flow unsteadiness is taken into account. As far as the unstable short-period oscillation is considered, which, in the quasistatic case, corresponds to $\hat{s} = 0.025 \pm 0.124i$, at convergence on $i\hat{\omega}$ we have $\hat{s} = -0.013 \pm 0.122i$.

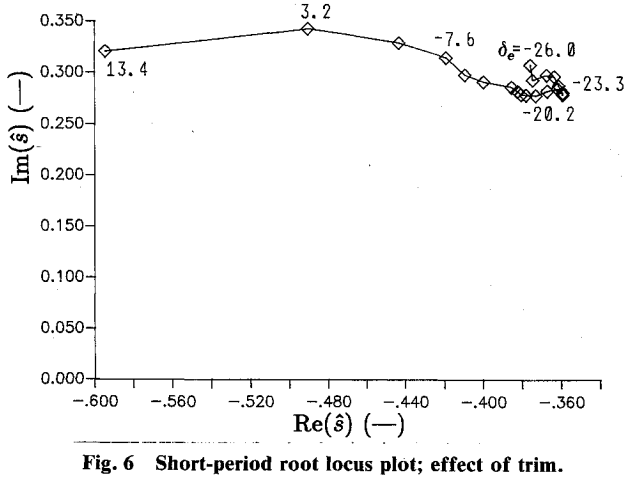

Fig. 6 Short-period root locus plot; effect of trim.

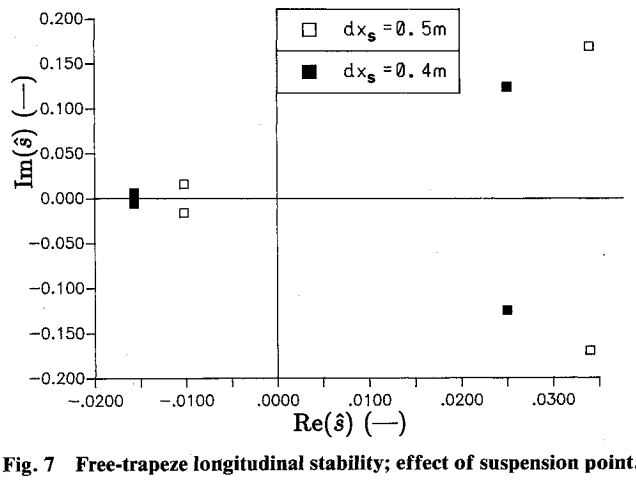

Fig. 7 Free-trapeze longitudinal stability; effect of suspension point.

Lateral Motion

When the homogeneous system associated with Eq. (13) is considered and the control equation is dropped, the eigenvalues of the lateral fixed-trapeze case can be calculated. They are reported in Fig. 9 for different values of the control angle δ. The values corresponding to a highly damped rolling convergence are not reported in the figure. The spiral motion is divergent for $\delta_e < -17$ deg, as is apparent when reference is made to the approximate expression of the spiral eigenvalue, i.e., $\hat{s}_{\text{spiral}} = -c_0/c_1$ (Ref. 6), where the first-order coefficient of the lateral characteristic equation c_1 is always positive and the zero-order coefficient c_0 is the left-hand side term in the lateral stability criterion [Eq. (18)].

The damping of the dutch-roll mode decreases with the angle of attack until, for $\delta_e > -7.1$ deg, we obtain a divergent motion. In this respect, the sign of the yaw-damping derivative C_{n_r} is crucial for the dutch-roll damping and C_{n_r}, as computed in the present test case, is positive at α_e larger than 4 deg due to the forward equilibrium position of the c.g. We should also note that, at low C_{L_e} flight conditions, high and somehow dubious variations of the computed lateral rotary derivatives vs α result in the present case as a consequence of the large displacements of the center of rotation of the system associated to the different equilibrium incidences (see Fig. 2c). However, we can conclude that the variable position of the center of rotation plays a significant role in the lateral stability, even from an aerodynamic point of view, and this should be carefully considered in wind-tunnel tests where, as a common assumption in the free-trapeze case takes, the suspension point is the rotation center.

The roots for the free-trapeze situation are as follows, at $\alpha_e = 14$ deg:

$$\hat{s}_1 = -2.78, \qquad \hat{s}_2 = 0.19, \qquad \hat{s}_3 = 0.011$$

$$\hat{s}_{4,5} = -0.16 \pm 022i, \qquad \hat{s}_6 = -0.26$$

where two divergent modes are shown to occur.

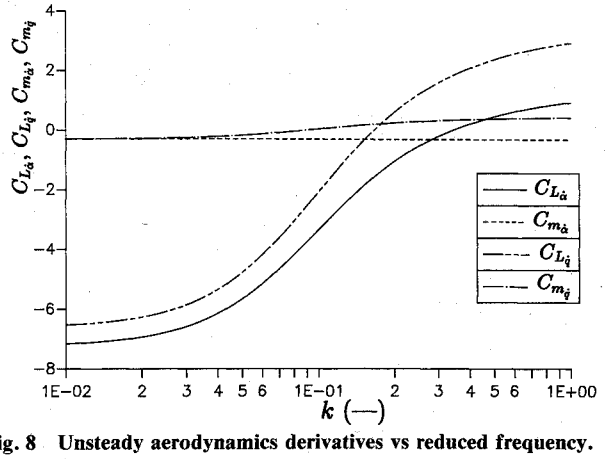

Fig. 8 Unsteady aerodynamics derivatives vs reduced frequency.

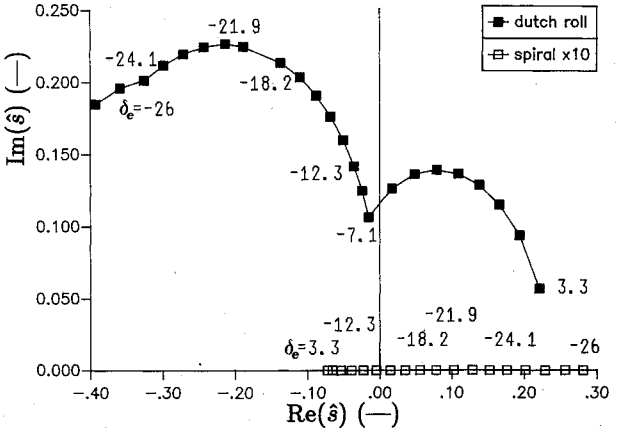

Fig. 9 Lateral root locus plot; effect of trim.

V. Conclusions

Some dynamics and control aspects of a typical, reference hang glider have been discussed. The assumed model of the hang glider, as a compound system made of wing and pilot, appears to extend and complete the work previously presented. The proposed formulation of the equations of motion and control provides a basis for future developments in the simulation of the glider flight. As a first step in the dynamic analysis, the stability characteristics have been shown to depend heavily on the trimmed flight conditions due to the variable position of the c.g. that is necessary for governing. Severe instabilities can arise, particularly in free-trapeze flight, and, in this respect, apparent mass and unsteady circulatory lift have a positive, damping effect. Attention is to be paid to the center of rotation of the system in evaluating the lateral rotary derivatives, particularly at low C_{L_e}, which corresponds to forward equilibrium positions of the pilot.

Appendix A: Evaluation of the Moments of Inertia

The moment of inertia about y is given by

$$\hat{I}_{y_e} = \hat{I}^W_{S_y} + \mu^P \hat{l}^2_S - (\hat{x}^{S2}_e + \hat{z}^{S2}_e)\mu^T \tag{A1}$$

where $\hat{I}^W_{S_y}$ is the constant moment of inertia of the wing about an axis parallel to y through point S. Analogously,

$$\hat{I}_{x_e} = \hat{I}^W_{S_x} + \mu^P(\hat{l}_S \cos\delta_e)^2 - \mu^T \hat{z}^{S2}_e \tag{A2}$$

$$\hat{I}_{z_e} = \hat{I}^W_{S_z} + \mu^P(\hat{l}_S \sin\delta_e)^2 - \mu^T \hat{x}^{S2}_e \tag{A3}$$

$$\hat{I}_{xz_e} = \hat{z}^S_e \int_{\mu^W} \hat{x}_e \, d\mu + \mu^P \hat{x}^P_e \hat{z}^P_e \tag{A4}$$

Appendix B: Unsteady Aerodynamic Derivatives

Consider a two-dimensional airfoil performing small pitching and plunging oscillations in an incompressible potential flow in the Laplace domain.[8] We have for the section lift and moment coefficients

$$\bar{C}_{L_s} = \left[C(s) + \frac{\hat{s}}{2}\frac{c}{\bar{c}}\right] C_{L_{\alpha s}} \bar{\alpha}_{¼} + \frac{\pi \hat{s}^2}{2}\frac{c^2}{\bar{c}^2}\bar{\theta} \tag{B1}$$

$$\bar{C}_{m_e} = -\frac{\pi}{4}\frac{c}{\bar{c}}\bar{\theta} - \pi\frac{c^2}{\bar{c}^2}\bar{\theta}\left[\frac{1}{16} + \frac{x}{c}\frac{1}{2}\right]\hat{s}^2 + C_{L_{\alpha s}}\left[C(s)\left(\frac{1}{4} + \frac{x}{c}\right) + \frac{x}{2c}\hat{s}\right]\bar{\alpha}_{¼} \tag{B2}$$

where

$$x = x_{c/4} - (x_{\text{c.g.}} - c/2) \tag{B3}$$

$$\bar{\alpha}_{¼} = \bar{\alpha} + \hat{x}_d \bar{\theta} \hat{s} \tag{B4}$$

and $\hat{x}_d = 2x/\bar{c}$ is the dimensionless distance between the three-quarter chord and the axis of rotation throughout the c.g.

For a harmonic airfoil motion, we may write

$$C(k_0) = F_0 + iG_0 = F_0 + ik_0\left(\frac{G_0}{k_0}\right) \tag{B5}$$

where F_0 and G_0 are the real and imaginary parts of the generalized Theodorsen's function, calculated for $k = k_0$. For k not too far from k_0, we write

$$C(k) = F_0 + ik\left(\frac{G_0}{k_0}\right) \tag{B6}$$

then

$$C(\hat{s}) = C_0 + \hat{s}C_1 \tag{B7}$$

where $C_0 = F_0$ and $C_1 = G_0/k_0$. $C(k)$ is expressed by Ref. 5 as

$$C(k) = \frac{0.5(ik + 0.135)(ik + 0.651)}{(ik + 0.0965)(ik + 0.4555)} \tag{B8}$$

Equation (B1) with Eqs. (B4) and (B7) is integrated over the semispan.[4] By taking the inverse Laplace transform of the resulting expression for the wing lift coefficient, we have

$$C_{L_\alpha} = \frac{2}{S} C_0 A_1 = C_0 C_{L_{\alpha_{st}}} \tag{B9a}$$

$$C_{L_{\dot\alpha}} = \frac{2}{S\bar c} A_2 (C_1 + 0.5) \tag{B9b}$$

$$C_{L_q} = \frac{2}{S\bar c} C_0 A_3 = C_0 C_{L_{q_{st}}} \tag{B9c}$$

$$C_{L_{\dot q}} = C_{L_{q_{st}}} (C_1 + 0.5) + \frac{\pi}{S\bar c^2} A_4 \tag{B9d}$$

and

$$A_1 = \int C_{L_{\alpha_s}} c \, dy, \qquad A_2 = \int C_{L_{\alpha_s}} c^2 \, dy$$

$$A_3 = \int C_{L_{\alpha_s}} \hat x_d c^2 \, dy, \qquad A_4 = \int c^3 \, dy$$

The same procedure, when Eq. (B2) is taken into consideration, gives

$$C_{m_\alpha} = (2/S\bar c) A_1 C_0 = C_{m_{\alpha_{st}}} C_0 \tag{B10a}$$

$$C_{m_{\dot\alpha}} = (2/S\bar c^2)[A_2 C_1 + (A_3/2)] \tag{B10b}$$

$$C_{m_q} = (2/S\bar c)[-(\pi/4\bar c) A_4 + C_0 A_5] = C_{m_{q_{st}}} C_0 - (\pi/2S\bar c^2) A_4 (1 - C_0) \tag{B10c}$$

$$C_{m_{\dot q}} = (2/S\bar c^2)[-\pi(A_6/\bar c) + C_1 A_7 + (A_8/2)] \tag{B10d}$$

where

$$A_1 = \int C_{L_{\alpha_s}} \left(\frac{1}{4} + \frac{x}{c}\right) c^2 \, dy, \qquad A_2 = \int C_{L_{\alpha_s}} \left(\frac{1}{4} + \frac{x}{c}\right) c^3 \, dy$$

$$A_3 = \int C_{L_{\alpha_s}} x c^2 \, dy, \qquad A_4 = \int c^3 \, dy$$

$$A_5 = \int C_{L_{\alpha_s}} \left(\frac{1}{4} + \frac{x}{c}\right) \hat x_d c^2 \, dy, \qquad A_6 = \int \left(\frac{1}{16} + \frac{x}{c}\frac{1}{2}\right) c^4 \, dy$$

$$A_7 = \int C_{L_{\alpha_s}} \left(\frac{1}{4} + \frac{x}{c}\right) \hat x_d c^3 \, dy, \qquad A_8 = \int C_{L_{\alpha_s}} x \hat x_d c^2 \, dy$$

References

[1]La Burthe, C., and Walden, S., "Flight Safety of Rogallo Hang Gliders. Theoretical and Experimental Study of the Flight Envelope," European Space Agency, ESA-TF 634, Feb. 1981.

[2]Kroo, I. M., "Aerodynamics, Aeroelasticity, and Stability of Hang Gliders," Ph.D. Thesis, Stanford Univ., Stanford, CA, May 1983.

[3]de Matteis, G., "Dynamics and Control of Hang Gliders," Internal Rept., Dept. of Mechanics and Aeronautics, Univ. of Rome La Sapienza, Rome, Italy, Oct. 1988.

[4]Carson Yates, E., "Modified-Strip-Analysis Method for Predicting Wing Flutter at Subsonic to Hypersonic Speeds," *Journal of Aircraft,* Vol. 3, No. 1, 1966, pp. 25–29.

[5]Venkatesan, C., and Friedmann, P. P., "New Approach to Finite-State Modelling of Unsteady Aerodynamics," *AIAA Journal,* Vol. 24, No. 12, 1986, pp. 1889–1897.

[6]Etkin, B., *Dynamics of Atmospheric Flight,* Wiley, New York, 1972, Chap. 5.

[7]de Matteis, G., and de Socio, L. M., "Nonlinear Aerodynamics of a Two-Dimensional Membrane Airfoil with Separation," *Journal of Aircraft,* Vol. 23, No. 11, 1986, pp. 831–836.

[8]Bisplinghoff, R. L., and Ashley, H., *Principles of Aeroelasticity,* Dover, New York, 1985, Chap. 6.